Regulatory networks specifying cortical interneurons from human embryonic stem cells reveal roles for CHD2 in interneuron development

Kesavan Meganathan[a], Emily M. A. Lewis[a], Paul Gontarz[a], Shaopeng Liu[a], Edouard G. Stanley[b], Andrew G. Elefanty[b], James E. Huettner[c], Bo Zhang[a], and Kristen L. Kroll[a,1]

[a]Department of Developmental Biology, Washington University School of Medicine, St. Louis, MO 63110; [b]Murdoch Childrens Research Institute, Royal Children's Hospital, Parkville, VIC 3052, Australia; and [c]Department of Cell Biology and Physiology, Washington University School of Medicine, St. Louis, MO 63110

Edited by Marianne Bronner, California Institute of Technology, Pasadena, CA, and approved November 14, 2017 (received for review July 17, 2017)

Cortical interneurons (cINs) modulate excitatory neuronal activity by providing local inhibition. During fetal development, several cIN subtypes derive from the medial ganglionic eminence (MGE), a transient ventral telencephalic structure. While altered cIN development contributes to neurodevelopmental disorders, the inaccessibility of human fetal brain tissue during development has hampered efforts to define molecular networks controlling this process. Here, we modified protocols for directed differentiation of human embryonic stem cells, obtaining efficient, accelerated production of MGE-like progenitors and MGE-derived cIN subtypes with the expected electrophysiological properties. We defined transcriptome changes accompanying this process and integrated these data with direct transcriptional targets of NKX2-1, a transcription factor controlling MGE specification. This analysis defined NKX2-1–associated genes with enriched expression during MGE specification and cIN differentiation, including known and previously unreported transcription factor targets with likely roles in MGE specification, and other target classes regulating cIN migration and function. NKX2-1–associated peaks were enriched for consensus binding motifs for NKX2-1, LHX, and SOX transcription factors, suggesting roles in coregulating MGE gene expression. Among the NKX2-1 direct target genes with cIN-enriched expression was *CHD2*, which encodes a chromatin remodeling protein mutated to cause human epilepsies. Accordingly, CHD2 deficiency impaired cIN specification and altered later electrophysiological function, while CHD2 coassociated with NKX2-1 at *cis*-regulatory elements and was required for their transactivation by NKX2-1 in MGE-like progenitors. This analysis identified several aspects of gene-regulatory networks underlying human MGE specification and suggested mechanisms by which NKX2-1 acts with chromatin remodeling activities to regulate gene expression programs underlying cIN development.

human embryonic stem cells | medial ganglionic eminence | cortical interneurons | NKX2-1 | CHD2

The mammalian cerebral cortex consists of two main categories of neurons, excitatory neurons that convey information to distant neurons within and outside the cortex and GABAergic cortical interneurons (cINs) that provide local inhibition to modulate excitatory neuron activity (1, 2). Interneuron loss or dysfunction during development alters the balance between neuronal excitation and inhibition, contributing to many neurodevelopmental disorders, including epilepsy (1–3).

cIN development begins with dorsoventral patterning of the telencephalon through regional transcription factor (TF) activities. While the cerebral cortex derives from the dorsal telencephalon, in the ventral telencephalon three progenitor domains, the medial, lateral, and caudal ganglionic eminences (MGE, LGE, and CGE, respectively) generate distinct neuronal types (1, 3–5). In rodents, the MGE provides the majority of cINs, which populate the cortex, hippocampus, and striatum. MGE progenitor specification is followed by differentiation, tangential neuronal migration to target locations, and maturation to acquire physiological properties. These processes are largely determined by cell-intrinsic activities (2). Notably, cIN development in rodents and primates differs significantly (6). During primate evolution, cINs increased in number, complexity, and proportion, relative to cortical excitatory neurons (7, 8). Likewise, the human cortex is twice as thick as that of the mouse, necessitating greater numbers of cIN progenitors. These differentiate over an extended gestational period, increasing their sensitivity to perturbation (7, 8).

Study of the molecular networks controlling human cIN development is limited by lack of access to fetal brain materials and inability to obtain expandable cIN progenitors or purify cINs from brain tissues. Therefore, approaches for modeling human cIN development in vitro are essential to define this developmental program and understand its disruption in disease. Here, we addressed these questions by refining protocols for directed differentiation of human embryonic stem cells (hESCs) into MGE-like progenitors and cIN-like neurons, obtaining efficient, accelerated production of mature cIN subtypes with the expected functional properties. We used this model to define transcriptome changes accompanying MGE specification and cIN differentiation and direct targets of the

Significance

In the human cerebral cortex, activities of excitatory neurons are balanced by local inhibition provided by cortical interneurons (cINs). Although disrupted cIN development contributes to neurodevelopmental disorders, molecular networks controlling this process were largely unknown. Here, we refined protocols for differentiating human embryonic stem cells into functional cINs. We defined gene-expression programs underlying cIN development and direct targets of the NKX2-1 transcription factor in this process, identifying potential regulators. These included *CHD2*, a gene mutated to cause human epilepsies. Accordingly, CHD2 deficiency impaired cIN development and altered later cIN function, while CHD2 and NKX2-1 could coregulate cIN gene expression by cobinding shared genomic regulatory regions. This work defines key features of both normal and disrupted cIN development.

Author contributions: K.M., and K.L.K. designed research; K.M., E.M.A.L., and J.E.H. performed research; S.L., E.G.S., and A.G.E. contributed new reagents/analytic tools; K.M., E.M.A.L., P.G., J.E.H., B.Z., and K.L.K. analyzed data; and K.M., J.E.H., and K.L.K. wrote the paper.

The authors declare no conflict of interest.

This article is a PNAS Direct Submission.

Data deposition: The data reported in this paper have been deposited in the Gene Expression Omnibus (GEO) database, https://www.ncbi.nlm.nih.gov/geo (accession no. GSE99937).

[1]To whom correspondence should be addressed. Email: kkroll@wustl.edu.

This article contains supporting information online at www.pnas.org/lookup/suppl/doi:10.1073/pnas.1712365115/-/DCSupplemental.

NKX2-1 TF during this process. In mice, NKX2-1 controls both MGE specification and cIN differentiation, with conditional loss of function resulting in MGE deficits, overproduction of alternate cell fates (e.g., LGE), and spontaneous seizures (9–11). During both murine and human neurodevelopment, NKX2-1 exhibits MGE-restricted expression (7, 8), while human *NKX2-1* mutations cause chorea, hypotonia, and dyskinesia (3, 12). Although NKX2-1 direct targets were recently defined in mouse MGE (13), in human cIN development they remained unknown.

Here, we integrated NKX2-1–associated genes in MGE-like progenitors with the MGE- and cIN-enriched transcriptome. This defined NKX2-1 direct target genes encoding known and previously unreported regulators of cIN migration, differentiation, and function and suites of transcriptional and epigenetic regulators that may comprise a gene-regulatory network mediating human MGE specification. Among these was CHD2, a member of the chromodomain helicase DNA-binding (CHD) family of chromatin-remodeling enzymes (14). Human mutations resulting in *CHD2* haploinsufficiency cause pediatric epilepsies involving refractory seizures, cognitive decline, and poor prognosis (14). As *CHD2* expression increased during cIN differentiation, we examined its requirements for this process, determining that NKX2-1 regulates *CHD2* expression by binding a *cis*-regulatory element (CRE) in the *CHD2* gene promoter, while CHD2 and NKX2-1 cobind some of the same CREs, and CHD2 promotes NKX2-1–dependent target gene transactivation. Accordingly, CHD2 knockdown (KD) and knockout (KO) revealed requirements in cIN differentiation and CHD2-dependent transcriptional programs, including regulation of human epilepsy genes, during this process. Together, these data provide a foundation for beginning to define the molecular basis of human cIN specification and differentiation and to identify how its dysregulation may contribute to neurodevelopmental disorders.

Results

Directed Differentiation of hESCs into MGE-Like Progenitors and cIN-Like Neurons. To generate hESC-derived ventral telencephalic-like neuroectoderm, MGE-like progenitors (hMGEs), and mature cIN-like neurons (hcINs) we used the hESC lines H9 and Hes3-NKX2-1$^{GFP/W}$, which has a GFP reporter knockin at the *NKX2-1* locus (15). Beginning with previously published protocols (16, 17), we tested many variables systematically, with goals of generating high percentages of hESC-derived hMGEs and driving their rapid, efficient differentiation into hcINs. Protocol modifications were tested with the NKX2-1–eGFP line to track frequencies of NKX2-1–expressing hMGEs, with further experimentation in H9 hESCs. Prior protocols differed in several respects, using either embryoid body (EB) or monolayer culture, inhibiting Wnt, BMP (ALK2/3), and TGF-β (ALK5) signaling with either recombinant proteins or small-molecule inhibitors, and combining these manipulations with either continuous or timed [day (d) 10–18] administration of the sonic hedgehog (SHH) agonist purmorphamine (16, 17). We tested these and other variables and obtained the highest frequency of NKX2-1–expressing progenitors by using EB culture, continuous purmorphamine treatment, and small-molecule inhibitors. In particular, EB approaches induced both NKX2-1–expressing progenitors and neurons expressing mature cIN subtype markers more efficiently than monolayer culture (Fig. S1*A*) and so were used for further experiments. Other parameters tested included starting cell numbers, time of Y-27632 withdrawal, time of EB plating for differentiation, and inclusion of a rosette selection purification step (Fig. S1*B*). The modified protocol used for all work below is schematized in Fig. 1*A* and is described in *Methods* and *SI Methods*.

We used the NKX2-1–eGFP hESC line to assess the kinetics of producing NKX2-1–expressing progenitors. During human fetal development, NKX2-1 is expressed specifically in the MGE from approximately gestational weeks 8–14, and NKX2-1–expressing GABAergic interneurons are also detected in the cortex in the third trimester, potentially following migration from the MGE (7). During directed differentiation in vitro, NKX2-1–eGFP expression was visible by d4–6, was strongly expressed in most cells by d12–15, and continued to be expressed through neuronal differentiation and maturation (d27–60) (Fig. S1*C*). More than 80% of cells expressed NKX2-1–eGFP by d15, suggesting that specification to an NKX2-1–expressing progenitor had occurred by then, with NKX2-1 expression at similar frequencies through d35 (Fig. 1*B*).

To further characterize neurons generated with this protocol, we performed immunocytochemistry (ICC) at d35. We observed high frequencies of cells expressing NKX2-1 (86.2 ± 1.9%), the ventral telencephalic markers ASCL1 (83.8 ± 1.6%) and OLIG2 (85.9 ± 1.6%), the ganglionic eminence (GE) marker DLX2 (83.9 ± 2.1%), the pan-telencephalon–enriched gene FOXG1 (67.4 ± 2.6%), and the neuronal markers DCX (65.6 ± 3.7%) and TUBB3 (69.8 ± 3.8%). These cells also efficiently expressed the GABAergic neuron markers GAD65/67 (65.5 ± 4.1 %) and GABA (74.4 ± 2.8%) (Fig. 1 *C* and *D*). We also performed ICC for CXCR4 (35.2 ± 2.7%), marking migrating neurons, CALB1 (38.8 ± 3.2%), marking GABAergic interneurons, and parvalbumin (PV; 37.7 ± 2.1%) and somatostatin (SST; 34.2 ± 1.4%), which mark the two major MGE-derived cIN subtypes (Fig. 1 *C*–*E*) (7, 18). By contrast, few cells were immunopositive for calretinin (CR), which predominantly marks a CGE-derived cIN subtype (Fig. S1*D*) (10). Few or no cells expressed Ki-67, which marks proliferating cells, NKX2-2, a diencephalon marker, RAX, a hypothalamic marker, or DARPP32, which marks LGE-derived striatal neurons (Fig. 1 *C* and *D*). Total numbers of immunopositive and scored cells are given in Table S1. Together, these results suggest that our modified protocol promotes the formation of MGE-like neural progenitors, which differentiate into GABAergic neurons expressing cIN markers, including PV or SST, which mark the two major subtypes of MGE-derived cINs. This constitutes higher percentages of cells expressing SST or PV than were previously observed without further coculturing (16, 17, 19).

Engraftment and Functional Characterization of hESC-Derived cIN-Like Neurons. We next tested the engraftment capacity and functional properties of these hcINs. We prepared hcINs for transplantation into murine brain, using polysialic acid (PSA)–neural cell adhesion molecule (NCAM) selection to remove residual proliferating cells, transducing neurons with a synapsin (SYN)–eGFP transgene (Fig. 2*A*), and transplanting them into either the adult hippocampus or neonatal cortex of NOD/SCID mice, observing engraftment 1 mo posttransplantation (Fig. 2 *B* and *C* and Fig. S1 *E* and *F*).

For electrophysiology, hcINs were prepared as above and then cultured on a rat cortical astrocyte feeder layer for ∼3 wk (Fig. 2*D* and *SI Methods*). hcINs developed voltage-gated and ligand-gated currents typical of CNS neurons. Under current clamp, hcINs fired action potentials (Fig. 2 *E* and *F*) and received spontaneous synaptic inputs (Fig. 2*G*), with most cells firing numerous spikes during prolonged depolarizing current pulses (Fig. 2*F*). Under whole-cell voltage clamp, depolarizing steps elicited an inward TTX-sensitive sodium current (Fig. 2*H*) and outward potassium currents that were blocked by a combination of tetraethyl ammonium and 4-aminopyridine (20). Agonists for excitatory and inhibitory neurotransmitter receptors, including kainate, NMDA, GABA, and glycine, evoked whole-cell currents when applied by local perfusion (Fig. 2*I*). Recordings revealed frequent spontaneous inhibitory postsynaptic currents (sIPSCs) that were blocked by the GABA receptor antagonist bicuculline methiodide (Fig. 2*G*), while evoked inhibitory postsynaptic currents (IPSCs) were relatively infrequent (3 of 31 cells tested in paired recordings) (Fig. 2*J*). Fig. 2*K* elaborates the electrophysiological properties observed, which suggest that these differentiation conditions result in hESC-derived neurons with the expected functional properties of GABAergic cINs.

Transcriptome Changes Accompanying Differentiation of hESCs. Our analysis above suggested that this directed differentiation protocol generated MGE-like progenitors that differentiated into neurons expressing GABAergic, cIN, and mature MGE-derived

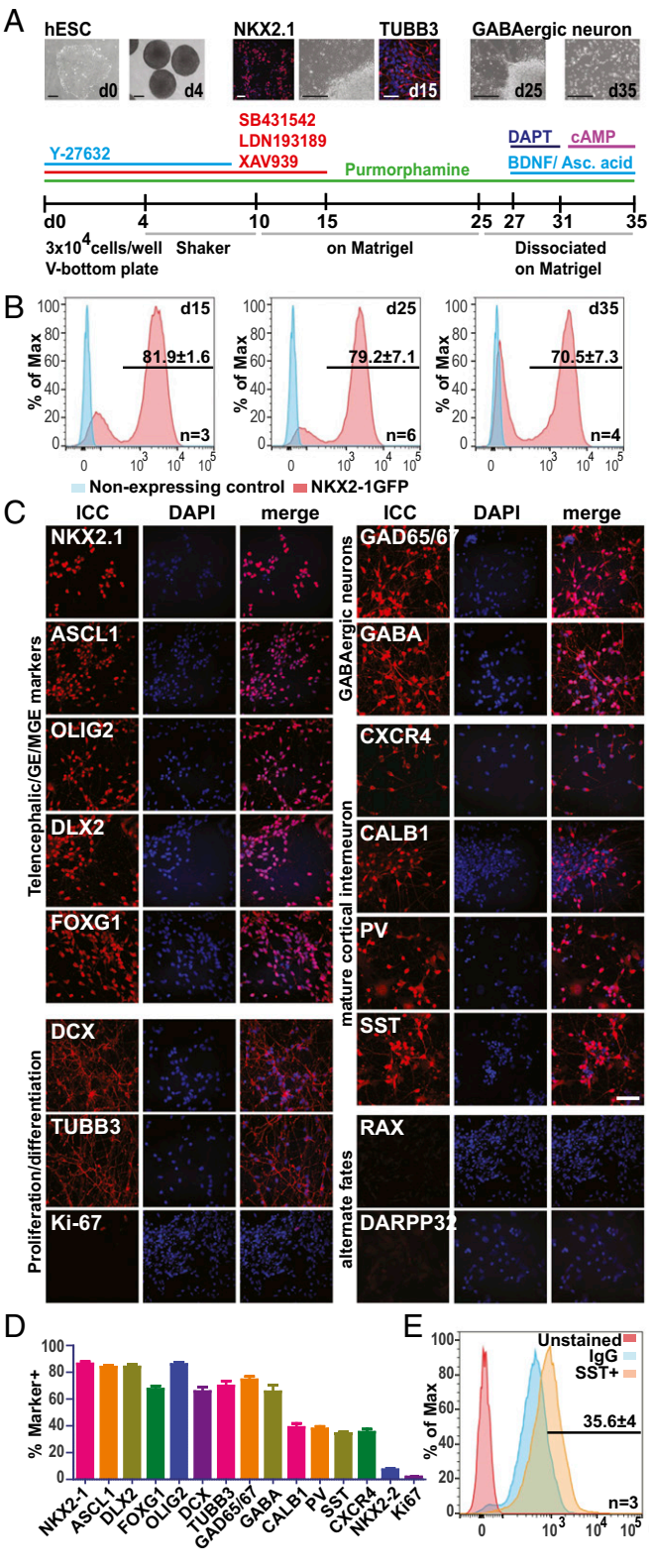

Fig. 1. Differentiation of hESCs into hcINs. (*A*) Scheme used, with representative markers or light microscopic images and days of treatment. (*B*) Representative FACS plots measuring cells expressing NKX2-1–eGFP reporter (red) and non-expressing cells (blue); the average percentage of eGFP-expressing cells ± SEM and biological replicates (*n*) are shown. (*C* and *D*) ICC at d35 with antibodies shown (*C*) and quantified (mean ± SEM) (*D*). (*E*) Representative FACS plot in d35 hcINs stained with SST antibody (yellow) or IgG control (blue) or unstained (red). The percentage of SST-immunopositive cells (mean ± SEM) is shown; $n = 3$. (Scale bars: *A*, 200 μm in brightfield images and 50 μm in fluorescence images; *C*, 50 μm.)

cIN subtype markers and exhibiting electrophysiological properties expected for cINs. Therefore, to comprehensively define the transcriptome changes accompanying this specification and differentiation process, we performed RNA-sequencing (RNA-seq) analysis at d0 (hESCs), d4, d15, d25, and d35. Stage-specific differentially expressed genes (DEGs) were defined by comparison with normalized expression at the prior time point, as described (*SI Methods* and Dataset S1), and were visualized by a multidimensional scaling plot (Fig. 3*A*). Replicates exhibited minimal variability, with the greatest change in DEGs from d0–4, when *NKX2-1* expression increased 280-fold, while the pluripotency marker *NANOG* decreased >1,000-fold (Dataset S1). Significant changes also occurred from d4–15 and d15–25, while fewer DEGs were observed from d25–35, suggesting potential stabilization of the neuronal state (Fig. 3*A*).

To assess whether this differentiation approach elicited gene-expression changes that accompany MGE specification and cIN differentiation during mouse and/or human development in vivo, we examined the temporal expression of genes that mark and regulate the formation of different forebrain regions and cell lineages in these data. During murine MGE specification, SHH signaling induces *NKX2-1*, *LHX6*, and *LHX8* predominantly in the MGE. This expression continues during cIN differentiation, while *NKX2-1* expression diminishes in maturing cINs (21). We observed a similar temporal sequence during hcIN differentiation: *NKX2-1* expression peaked at d15, with continued expression to d35, while *LHX6/8* expression began at d15 and increased through d35 (Fig. 3*B*). *ASCL1* and *OLIG2* mark the ventral forebrain in mouse and were most highly expressed from d15–25 and were reduced at d35 here. *DLX1*, *DLX2*, and *DLX5* mark the GEs in vivo and exhibited enriched expression from d14–35, as did the general anterior neural or forebrain markers *FOXG1*, *OTX2*, *SIX3*, and *SIX6* and neuronal markers *SYP* and *TUBB3*. By contrast, the dorsal telencephalic markers *EMX1*, *EMX2*, and *PAX6* were never expressed during differentiation (Fig. 3 *B* and *C*).

We also examined markers of later cell lineages. At d35 neurons expressed markers of GABAergic neurons (*GAD1/2* and *SLC32A1*/*SLC6A1*, required for GABA transport) (Fig. 3*C*) and mature cIN subtype markers, including the neuropeptides *SST* and *NPY*, but not *VIP*, which is expressed in CGE-derived interneurons (Fig. 3*D*), while expression of genes associated with neural or cIN migration (*CXCR4*, *ARX*, *DCX*, *NRN1*, *RELN*) was enriched from earlier time points. We also evaluated markers of other cell lineages, including *RAX*, a prospective forebrain and hypothalamic marker, *NKX2-2*, a diencephalic marker, and *DARPP32*, a striatal neuron marker. These exhibited transient, low-level expression during neural induction, which did not persist to later stages (Fig. 3*D*).

Based upon marker expression, this in vitro differentiation protocol yields ventral neuroectoderm of forebrain character by d4, neural progenitors expressing MGE markers most highly at d15 (with some persisting to later stages), and neurons expressing markers of cIN differentiation, function, and MGE-derived cIN subtype identity at d35. Therefore, we comprehensively characterized gene-expression profiles accompanying these developmental transitions by *k*-means clustering, based upon z-scores of expression across all data (Fig. 3*E*), to define major gene-expression changes accompanying the transition from a ventral telencephalic-like state. This analysis yielded nine clusters of DEGs (Fig. 3*F* and Fig. S2*A*). Of particular interest were clusters 1 and 7, in which genes exhibited greater than fourfold increased expression from d4–15 (Fig. 3*F*). Based upon marker gene expression, genes in these clusters significantly increased in expression during specification of ventral telencephalic neuroectoderm to an MGE progenitor-like state. Cluster 4 also exhibited greater than fourfold enrichment at later time points relative to d4, but this was only seen by d25–35 (Fig. 3*F*).

Gene Expression Signatures of MGE-Like Progenitors and cIN-Like Neurons and Comparison with Gene Expression in Human Fetal Brain. We performed gene ontology (GO) analysis on the *k*-means clusters highlighted above. Clusters 1 and 7 are enriched for GO terms related to early neurodevelopment (neurogenesis, axonal

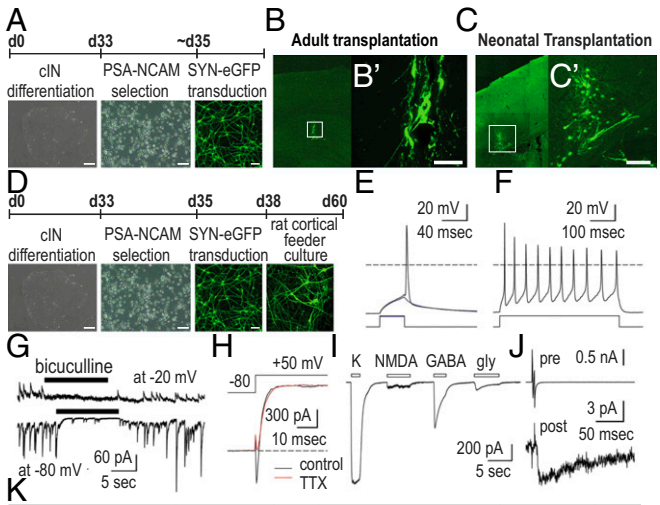

K

Parameters	Mean+/-sem	#cells	Parameters	Mean+/-sem	#cells
Capacitance (pF)	34.4 +/- 1.5	168	Max # of spikes	5.9 +/- 0.3	109
Input Resistance (GOhm)	0.9 +/- 0.06	168	Max 1st frequency (hz)	16.1 +/- 0.6	97
Resting Potential (mV)	-41.4 +/- 0.8	141	Max instantaneous Freq (hz)	12.4 +/- 0.5	97
Rheobase (pA)	19.2 +/- 2.3	109	Peak I Na (nA)	-2.0 +/- 0.1	134
1st spike threshold (mV)	-39.1 +/- 0.5	109	Vm for peak I Na (mV)	-26.9 +/- 0.9	134
1st spike amplitude (mV)	28.6 +/- 1.8	109	I Na at 0 mV	-1.2 +/- 0.08	134
1st spike halfwidth (msec)	5.5 +/- 0.4	109	I K at 0 mV	0.45 +/- 0.02	134

Fig. 2. Electrophysiology and engraftment of hcINs into the murine adult and neonatal brain. (*A–C*) Scheme: SYN–GFP–expressing hcINs (after PSA–NCAM selection) (*A*) were transplanted into the hippocampus (CA3) of adult mice (*B*) (*B′* shows the boxed region in *B*) or cortex of postnatal d2 NOD/SCID mice (*C*) (*C′* shows the boxed region in *C*). Images in *B* and *C* were taken 30 d posttransplantation. The "scan slide" mode in the MetaMorph software of the Olympus confocal microscope was used to assemble a composite view of the whole brain slice from several individual images. (*D*) Scheme: SYN–GFP–expressing hcINs (after PSA–NCAM selection) were cocultured on rat cortical astrocyte feeders for 3 wk before electrophysiology. (Scale bars: 100 μM in *A*, *C*, and *D*, 50 μM in *B′*) (*E*) Sub- and suprathreshold stimulation by injection of depolarizing current (52 and 56 pA for 40 ms). (*F*) Multiple action potentials during injection of depolarizing current (56 pA for 800 ms). (*G*) sIPSCs recorded at −80 and −20 mV are inhibited by exposure to 100 μM bicuculline methiodide (black bars). (*H*) Whole-cell currents recorded during a voltage step from −80 to +50 mV in control conditions (black trace) and with 0.5 μM TTX (red trace). (*I*) Currents evoked by exposure to 100 μM kainate (K), NMDA, GABA, and glycine (gly). (*J*) Evoked IPSCs elicited by a presynaptic voltage step. (*K*) Electrophysiological properties of hESC-derived hcINs (mean ± SEM).

guidance) (Fig. 4*A*). Among these genes, the GO gene subset for nervous system development (181 genes) includes many TFs with roles in neurogenesis and ventral telencephalon/GE/MGE specification (Fig. 4*B*). These clusters also include long noncoding RNAs with known or potential roles in neurodevelopment and genes with roles in axonal guidance and neuronal migration (examples are given in Table S2; all cluster 1 and 7 genes are given in Dataset S1*F*). Together, these data support an MGE-like character for genes with this enrichment profile and encourage future efforts to mine these data to identify regulators of MGE specification. Cluster 4 genes exhibited increased expression at d25–35 but not at d15, reflecting expression of known genes involved in cIN differentiation, function, and subtype identity. This cluster was enriched for GO terms associated with synaptogenesis, synaptic neurotransmission, and psychiatric disorders (Fig. 4*C*), including a distinct group of genes involved in neuronal guidance and genes that control GABAergic neurotransmission and maintain a mature neuronal state (Fig. 4*D* and Table S2 and Dataset S1*G*).

We also compared z-scores of transcript enrichment in our d15 hMGEs with relative regional transcript enrichment in postconception week 8–9 human brain (Fig. 4*E*). This revealed substantial similarity of d15 hMGE-enriched transcripts and fetal MGE and less similarity with other 8–9 wk or second–third trimester fetal brain structures (Fig. 4*E*). Together, these data suggest that hMGE specification mimics many aspects of regionally enriched gene expression in wk 8–9 MGEs in vivo, providing an experimentally manipulable context for studying molecular regulation of this developmental program.

NKX2-1 Direct Targets Regulating Specification of hMGE-Derived Cortical Interneurons. NKX2-1 is expressed in the MGE and MGE-derived cINs in both mouse and human and is required for both MGE specification and cIN differentiation in mouse (9–11). To define gene regulatory networks through which NKX2-1 may directly control these processes during human MGE specification, we identified its direct targets by performing NKX2-1 ChIP-sequencing (ChIP-seq) in d15 hMGEs (*Methods* and *SI Methods*). NKX2-1 chromatin enrichment was compared with IgG controls,

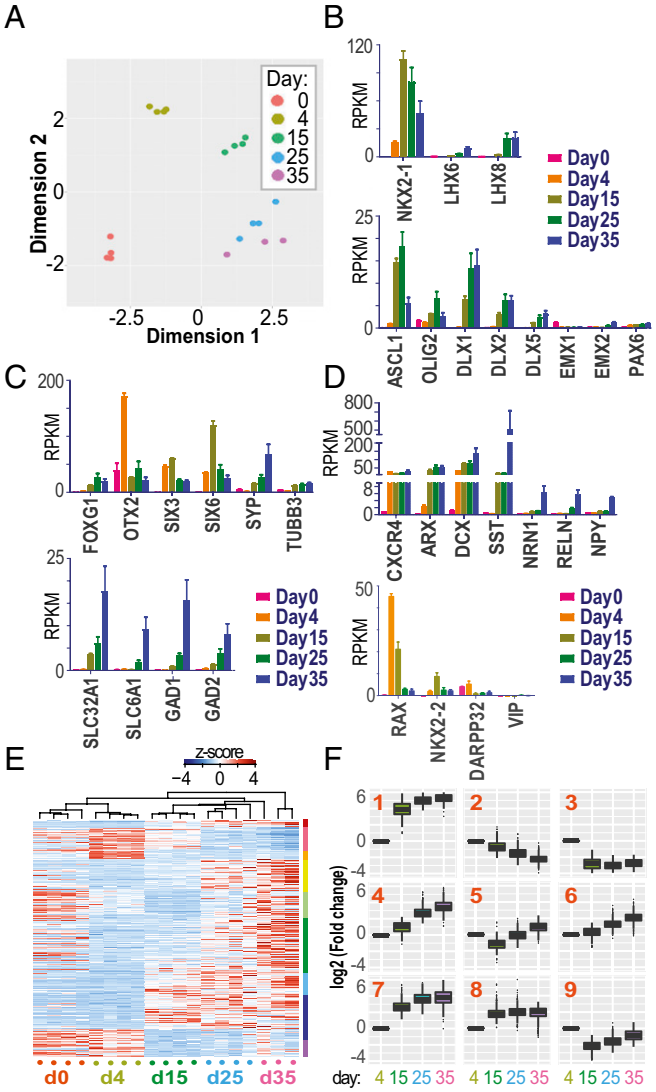

Fig. 3. Transcriptome changes accompanying hESC–hcIN differentiation determined by RNA-seq during differentiation, with samples collected as indicated. (*A*) Multidimensional scaling plot. (*B–D*) Average reads per kilobase of transcript per million reads mapped (RPKM) values for the expression of genes marking MGE, ventral or dorsal telencephalic neuroectoderm (*B*), anterior neuroectoderm and neurons/GABAergic neurons (*C*), and cIN migration/maturation and alternate cell lineages (*D*). (*E*) *k*-Means clustered data based upon expression *z*-scores. (*F*) *k*-Means clusters, as a log2 change versus d4, defining enriched clusters accompanying hMGE specification and hcIN differentiation.

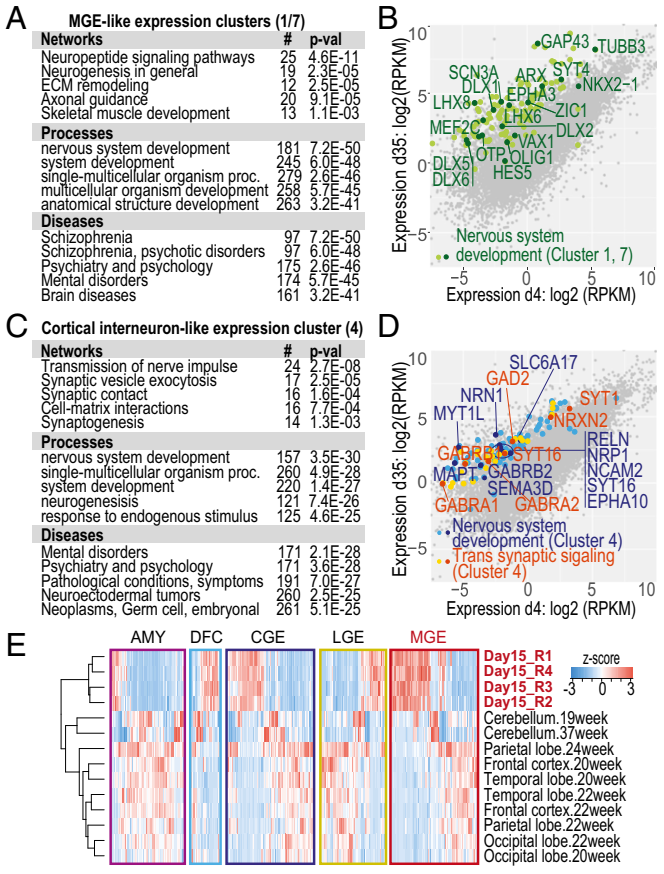

Fig. 4. Gene-expression profiles for d15 hMGEs and d35 hcINs. (*A*–*D*) *k*-Means clusters 1 and 7 (*A* and *B*) and cluster 4 (*C* and *D*) exhibited more than fourfold increased expression from d4–15 (clusters 1 and 7) or d4–35 (cluster 4). Enriched GO terms (*A* and *C*) and genes (*B* and *D*) in these clusters are shown. (*E*) Z-scores of relative expression at d15 (replicates = R1–4) compared with regional expression in fetal brain at 8–9 wk (*x* axis) and 19–37 wk (*y* axis) postconception. AMY, amygdala; DFC, dorsolateral prefrontal cortex.

defining 4,867 peaks with significant, reproducible enrichment (Dataset S2). About one quarter of these NKX2-1–bound sites (23%) were within 2 kb of the transcription start site (TSS), another quarter (23%) were 2–10 kb from the TSS, and the remainder mapped to locations >10 kb from the nearest TSS (Fig. 5*A* and Fig. S2*B*), with 62% of peaks overlapping the gene body, over 20% at the promoter, 18% in CpG islands, and 9% in brain-specific superenhancers (Fig. 5*B*). To test whether d15 was an appropriate time point for ChIP analysis, we analyzed the temporal expression of MGE and alternate fate markers more precisely (Fig. S2*C*). Optimal expression of many GE/MGE markers was observed after d12, while expression of alternate cell fate markers was reduced after d15, suggesting that d15 is an appropriate time point to identify NKX2-1 direct targets involved in MGE specification. We also validated several NKX2-1–enriched peaks by ChIP-qPCR at d4, d15, and d35. All genes were enriched for NKX2-1 binding at d15, but enrichment varied at the other time points (Fig. S2*D*). Therefore, while NKX2-1 targets relevant to hcIN differentiation (e.g., *SYT1*) (Fig. S2*D*) may also be enriched at later time points, d15 NKX2-1 enrichment appears to select for many targets involved in MGE specification.

To understand the relationship between NKX2-1 binding in hMGEs and regulation of gene expression, we assigned each peak to the nearest TSS (Dataset S2) and assessed the expression of the associated genes. Of the 1,000 NKX2-1–associated genes that changed expression by more than fourfold from d4 to d15, 59% (590 genes) increased in expression during MGE specification, suggesting a possible role for NKX2-1 in promoting their expression, while the rest (410 genes; 41%) had diminished expression (Fig. 5*C*). As shown previously, *NKX2-1* is expressed from ∼d4, peaks at d15, and is maintained during differentiation. As NKX2-1 can act as either a transcriptional activator or repressor in other contexts (22, 23), NKX2-1–associated genes with increased expression from d4 to d15 or d35 could potentially be direct targets of NKX2-1–dependent transactivation, while some NKX2-1–associated genes with low or diminished expression here may be targets of NKX2-1 repression (e.g., to block gene expression associated with alternate fates, such as LGE- or dorsal telencephalon-enriched genes). However, these changes in expression could also be independent of direct NKX2-1 regulation. GO analysis supports distinct roles for these sets of NKX2-1–associated genes, with NKX2-1–bound genes with increased expression from d4–15 involved in neurogenesis, synaptogenesis, axonal guidance, and psychiatric disorders, while

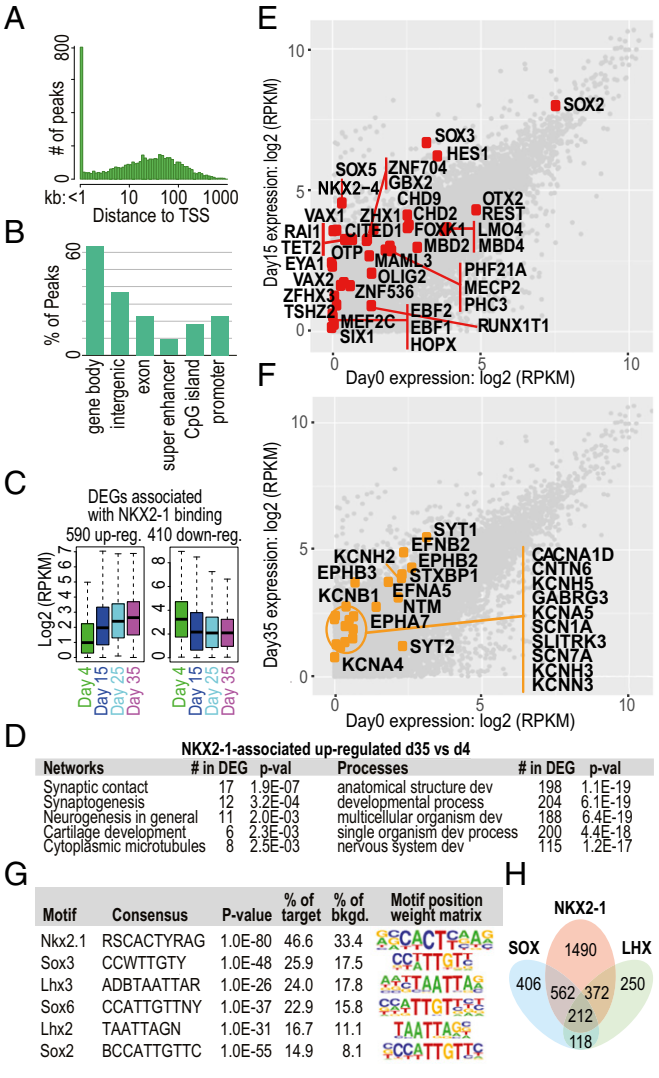

Fig. 5. Integrating NKX2-1 genome-wide association and enriched gene expression in hMGEs and hcINs. (*A*) Distance from NKX2-1 peak locations to the nearest TSS. (*B*) NKX2-1 peaks intersected with annotated genomic features. (*C*) Integration of NKX2-1 binding with log2 fold changes in expression for DEGs from d4–35 vs. d0. (*D*) Top GO terms for NKX2-1–associated genes with greater than twofold increased expression at d35 vs. d4. (*E* and *F*) NKX2-1–associated genes with enriched expression at d15 (*E*) or d35 (*F*). (*G*) Top consensus binding motif sequences enriched in NKX2-1–associated peaks. (*H*) Numbers of NKX2-1–bound peaks with each motif.

those with increased expression through d35 are also involved in later aspects of neuronal function (synaptic transmission, synaptic plasticity) (Fig. 5*D* and Dataset S2). Conversely, many NKX2-1–associated genes with diminished expression from d4 to d15 or d35 were involved in general cellular and developmental processes (e.g., cell cycle regulation, epithelium development, chromosome organization) (Dataset S2).

We focused on NKX2-1–associated genes with hMGE-enriched expression. These include many TFs that promote anterior or general neural identity, ventral telencephalon specification, cIN development, neurogenesis, or other neurodevelopmental functions, as well as TFs with no known role in neurodevelopment (Fig. 5*E* and Table S2). These data support a major role for NKX2-1 in regulating other TFs and suggest a transcriptional regulatory network downstream of NKX2-1 in MGE specification. Some NKX2-1–associated genes exhibit increased expression during both hMGE specification and hcIN differentiation. Many of these control cIN migration, axonal guidance, synaptogenesis, and synaptic neurotransmission and plasticity (Fig. 5*F* and Table S2). These include GABAA receptors, sodium, potassium, and calcium channels, and other genes involved in synaptic development and function (Table S2). Mutations in several of these genes result in epilepsy (*KCNB1*, *SCN1A*, *STXBP1*) (Fig. 5*F* and Dataset S2). This supports a role for NKX2-1 in regulating targets involved in cIN differentiation and function. NKX2-1 also associates with many other gene classes, including natural antisense transcripts and other long noncoding RNAs (examples are given in Table S2). These represent putative regulators of cIN development to be explored in future studies.

TF Consensus Binding Motif Enrichment in NKX2-1–Associated CREs. Using NKX2-1–associated peak sequences, we performed de novo motif discovery to identify the most highly enriched TF consensus binding motifs (*Methods*). An NKX2-1 consensus binding motif was the most frequently found (47% of peaks) (Fig. 5 *G* and *H*). This motif frequently co-occurred with motifs predicted to be bound by LHX (LHX2/3) or SOX (SOX2/3/6) TFs, which were each present in 15–25% of the NKX2-1–bound peaks (Fig. 5*G*); 1,264 peaks contained more than one type of motif (Fig. 5*H*). TFs that recognize these motifs and can regulate neural or cIN gene expression are expressed during hMGE specification and hcIN differentiation (Fig. 6*A*). SOX2/3 can transactivate neural gene expression, while NKX2-1 promotes MGE specification, and NKX2-1, LHX6, and SOX6 promote cIN differentiation. Accordingly, *SOX2/3* expression is most highly enriched in d4 ventral neuroectoderm, while *NKX2-1* peaks at d15 and persists through d35, and *SOX6* and *LHX6* are expressed from d15–35 (Fig. 6*A*).

SOX2/3/6 consensus motifs were highly enriched in NKX2-1–bound peaks, suggesting that SOX TFs might cobind these genomic locations with NKX2-1. Therefore, we compared our NKX2-1–binding data for hMGEs to ChIP-seq data for SOX2 in human neural progenitor cells (NPCs) (24). Approximately 20% of our NKX2-1–bound peaks intersected with sites of SOX2 binding (991 SOX2-bound peaks intersecting the 4,867 NKX2-1–bound peaks), supporting a potential coregulatory role. We focused on the subset of 299 peaks predicted to be cobound by both NKX2-1 and SOX2 and associated with genes with a greater than twofold expression change between d0–35 of hcIN differentiation. Of these, 81% (243) exhibited increased expression, and this gene set was highly enriched for genes involved in neural development (Fig. 6*B*). The much smaller set of predicted cobound genes with diminished expression was instead involved in general cellular functions (signaling, cell cycle, chromatin) (Fig. 6*C*).

We tested whether SOX2 and NKX2-1 could cobind the same putative CREs in hMGEs by selecting five CREs predicted to be bound by both TFs that also contained NKX2-1 and SOX consensus motifs (Fig. 6*D*). Expression of each CRE-associated gene increased during hESC–hMGE specification (Fig. 6*E*). SOX2 binding was highly enriched at each NKX2-1–bound putative CRE, supporting the hypothesis that NKX2-1 and SOX TFs may

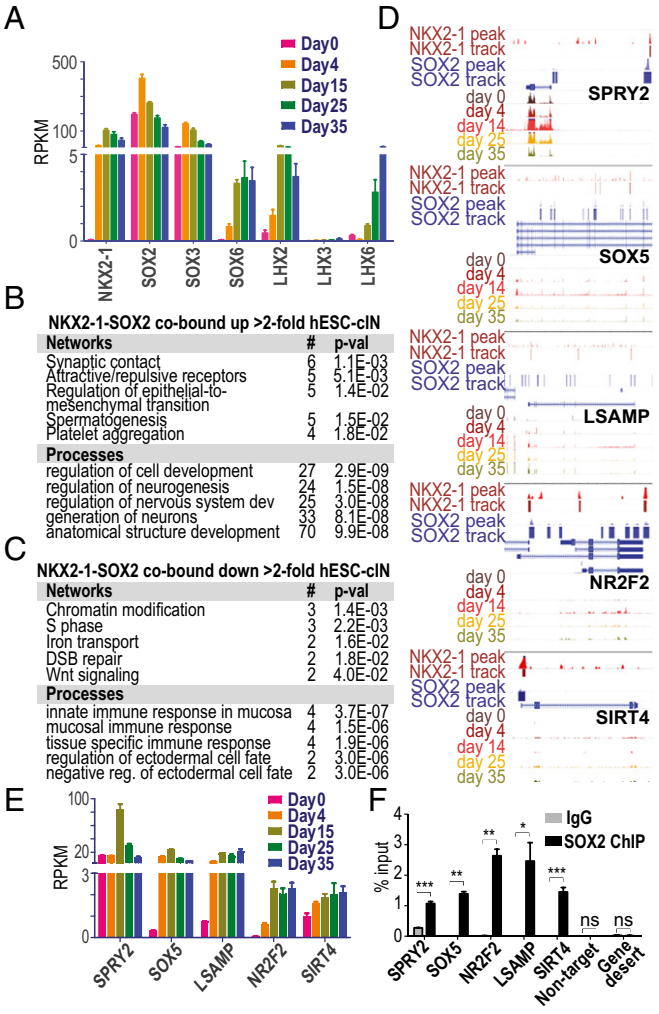

Fig. 6. NKX2-1 and SOX2 coassociate with putative CREs in hMGEs. (*A*) Expression profiles of TFs that recognize NKX2-1 peak-enriched consensus motifs (average RPKM). (*B* and *C*) Intersecting NKX2-1–bound peaks in hMGEs and SOX2-bound peaks in human NPCs (GSE69479) were mapped to the nearest TSS. Putative cobound-peak–associated genes with greater than twofold increased (*B*) or decreased (*C*) gene expression on d35 vs. d0 were analyzed for GO enrichment. (*D*) Examples of intersecting NKX2-1 and SOX2 peaks. (*E*) Expression profiles of these genes. (*F*) SOX2 enrichment, detected by ChIP-qPCR, in hMGEs at predicted cobound locations in *D*. Data are the average of $n = 3$ independent biological replicates. $*P < 0.05$, $**P < 0.01$, $***P < 0.001$ (unpaired Student's *t* test); ns, not significant.

cobind some CREs in hMGEs (Fig. 6*F*). We also found that co-overexpression (co-OE) of NKX2-1 and SOX2 could regulate reporter expression driven by these CREs in a luciferase assay, while this activity was lost upon mutation of the NKX2-1 consensus binding motifs in each CRE (Fig. S3*A*). Therefore SOX TFs could potentially contribute to NKX2-1–mediated regulation of hMGE gene expression through NKX2-1 and SOX2/3/6 coassociation at these CREs.

CHD2 Is a Direct Target of NKX2-1, and CHD2 Deficiencies Dysregulate the Program That Specifies cIN-Like Neurons. Interneuron dysfunction during development contributes to many neurodevelopmental disorders, including epilepsy (1–3). Therefore we sought to utilize this cIN model to identify regulators of cIN development implicated in neurodevelopmental disorders. As NKX2-1 controls cIN specification and differentiation, we examined the overlap between NKX2-1 direct targets with hcIN-enriched expression and annotated human epilepsy genes (Epi4K database; epi4kdb.org/).

Among these, we focused on *CHD2*, as haploinsufficiency following mutation or deletion of one allele of *CHD2* causes epileptic encephalopathies and, in some cases, autism spectrum disorders. Our ChIP-seq data defined an NKX2-1–bound putative CRE in hMGEs near the *CHD2* gene promoter (Fig. 7*A*). This CRE could drive luciferase reporter expression in hMGEs (Fig. 7*B*). NKX2-1 overexpression (OE) further increased reporter expression, while mutating the NKX2-1 motif in this CRE reduced reporter to baseline levels, even in the presence of overexpressed NKX2-1 (Fig. 7*B*). These data suggest that NKX2-1 binding to this CRE could promote *CHD2* expression (Fig. 7*B*). *CHD2* expression increased during hcIN differentiation (Fig. 7*C*), and CHD2 protein was enriched in nuclei of hcINs (Fig. 7*D*), supporting a role in this process. Therefore, we used two lentiviral shRNA constructs that reduce CHD2 levels to ∼50% of wild-type (CHD2 KD) to mimic haploinsufficiency seen in human patients (Fig. S3*B*).

To assess CHD2 requirements for hMGE specification, we conducted CHD2 KD in hESCs and performed RNA-seq analysis in d15 hMGEs. Differentially regulated genes in CHD2 KD versus nontarget control hMGEs are shown in Dataset S3. CHD2 KD reduced the expression of genes involved in neurogenesis, synaptogenesis, and neurotransmission, including potassium and sodium channels, and genes associated with neurological disorders, while genes up-regulated upon CHD2 KD were instead involved in adhesion and nonneural fate acquisition (Fig. 7*E*). Genes with reduced expression in the CHD2 KD include TFs involved in neurogenesis and hcIN specification, regulators of synaptogenesis, sodium channels, potassium channels, and genes required for potassium channel clustering (*CNTN2*, *CNTNAP2*) (Fig. 7*F* and Table S2 and Dataset S3). All CHD2-dependent synaptic and channel-related genes shown in Table S2 are also human epilepsy genes (Dataset S3), suggesting that their altered expression upon CHD2 deficiency could contribute to disrupted neuronal development or function underlying the epileptic phenotype.

To further test CHD2 requirements in hcIN differentiation, we generated hESC clonal lines with biallelic *CHD2* gene disruption (CHD2 KO) (*Methods*, *SI Methods*, and Fig. S3 *C* and *D*). These hESC lines did not exhibit altered expression of pluripotency, proliferation, or apoptotic markers or changes in EB size or morphology during early neural specification (d0–4) (Fig. S4). We assessed whether CHD2 loss affected cIN differentiation and gene expression by RT-qPCR and ICC in d15 hMGEs, focusing on genes with reduced expression in the KD RNA-seq data. Consistent with CHD2 KD, CHD2 KO reduced the levels of many of the same genes encoding TFs, potassium channels, and GABAergic neuronal markers (Fig. 7*G*). TUBB3 immunostaining at d15 suggested that some of these gene-expression changes involved delayed or impaired differentiation, as the CHD2-KO cells exhibited fewer TUBB3-expressing neurons with shorter neurites (Fig. 7 *H*–*J*) and reduced expression of the channel gene *HCN4* (Fig. 7 *H* and *I*).

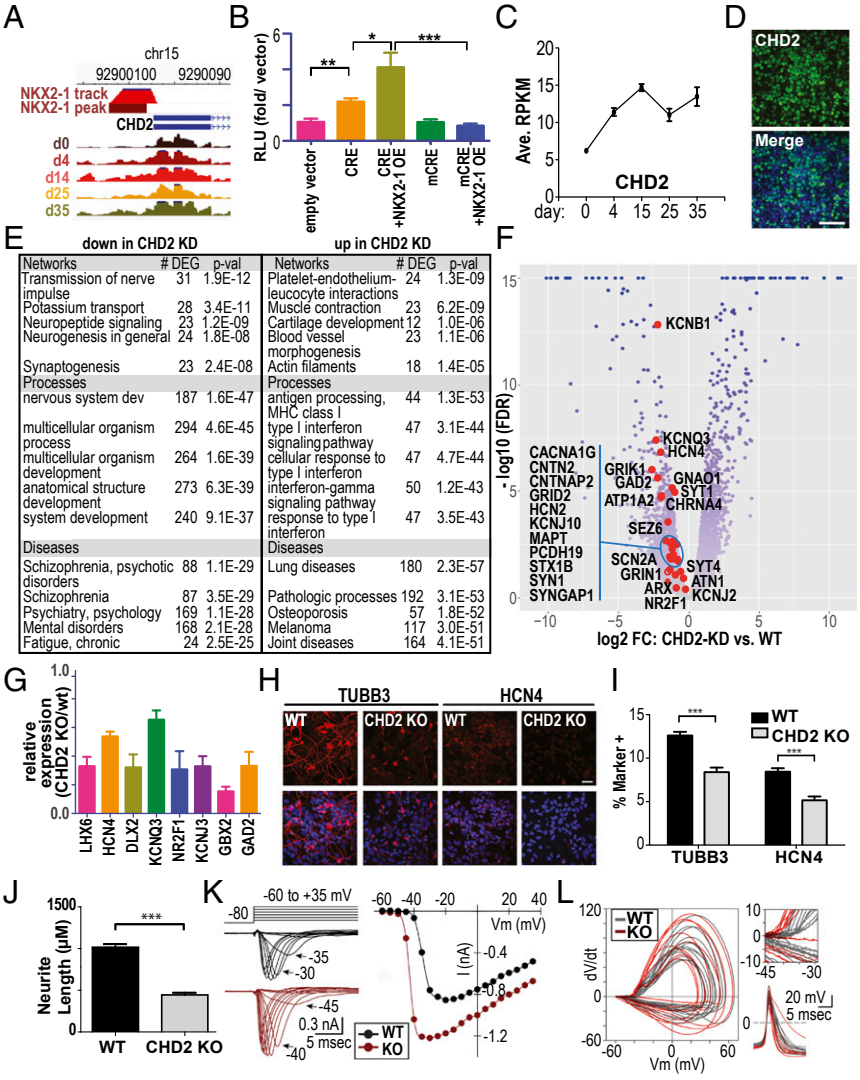

Fig. 7. Regulation of *CHD2* expression by NKX2-1 and CHD2 requirements for cIN development. (*A*) An NKX2-1–bound putative CRE was defined at the CHD2 promoter. (*B*) This CRE drives luciferase expression in hMGEs, while NKX2-1 OE further stimulates expression, and mutating the NKX2-1 consensus motif (mCRE) reduces expression to baseline. Average fold change of relative luciferase units (RLU) versus empty vector ($n = 3$; each replicate was performed in quintuplicate). (*C*) *CHD2* expression from d0–35. (*D*) CHD2 and DAPI (blue) ICC at d35. (*E* and *F*) RNA-seq analysis of CHD2-KD versus control shRNA-transduced hMGEs. (*E*) GO analysis of genes with greater than twofold decreased (down) or increased (up) expression in CHD2-KD versus control hMGEs. (*F*) Differentially regulated genes, with some highlighted. (*G*) Genes with reduced expression in the CHD2-KD RNA-seq were also diminished in hMGEs with biallelic CHD2-KO vs. wild-type hMGEs. (*H*–*J*) CHD2 KO reduced TUBB3 and HCN4 immunopositive cells (*H* and *I*) and neurite length (*J*). (*K*) Currents mediated by TTX-sensitive sodium channels during steps from a holding potential of −80 mV to test potentials ranging from −60 to +35 mV. Traces were obtained by subtracting currents recorded during exposure to TTX from currents recorded in control external solution without TTX. Peak inward current is plotted as a function of test potential for wild-type (black traces) and KO (red traces) cells. (*L*) Phase plots of action potentials from 13 wild-type (gray traces) and nine KO (red traces) neurons. The initial increase in dV/dt occurs at more negative membrane potentials in KO cells, indicating a difference in action potential threshold. (*Upper Right*) The inset is plotted on expanded scales. (*Lower Right*) The action potentials are aligned at the point of maximal upslope. In *B*, *I*, and *J*, $^{*}P < 0.05$, $^{**}P < 0.01$, $^{***}P < 0.001$ (unpaired Student's *t* test). (Scale bars in *D* and *H*: 50 μM.)

We also characterized the electrophysiological properties of both cortical excitatory neurons (generated as described in *SI Methods*) and wild-type hcINs with versus hcINs with biallelic CHD2 KO. By d35, CHD2-KO hcINs did not exhibit gross deficiencies in neuronal marker or cIN gene expression, suggesting that CHD2 loss delayed but did not block differentiation. However, while the excitatory neurons did not exhibit significant electrophysiological differences upon CHD2 KO, CHD2-KO hcINs displayed a significantly lower threshold for action potential firing, larger peak sodium current, and more negative voltage for peak sodium current than wild-type cells (Fig. 7 *K* and *L* and Table S5), suggesting developmental and/or continued CHD2 requirements for normal hcIN electrophysiological function.

Coregulation of Gene Expression by NKX2-1 and CHD2 in MGE-Like Progenitors. About 1/10th (9.6%; hypergeometric P value = 2.0×10^{-61}) of the CHD2-regulated genes were also NKX2-1–associated in hMGEs, suggesting that CHD2 might coregulate some of the NKX2-1 transcriptional program. During myogenesis, CHD2 can interact with the MyoD TF and contributes to MyoD-dependent activation of muscle differentiation gene expression (25), suggesting the potential for analogous CHD2 roles during neural development. To test whether such coregulation could occur, we focused on several candidate NKX2-1–associated putative CREs (Fig. 8*A*). The associated genes exhibit distinct temporal expression, with *ZIC1* and *SPRY1* expression enriched in hMGEs and cINs relative to hESCs, while *PAX2* expression is enriched in ventral telencephalic neuroectoderm at d4 but is reduced in hMGEs (Fig. 8*B*). ChIP-qPCR revealed CHD2 enrichment at all three NKX2-1–bound putative CREs but not at unrelated genomic locations used as controls [gene desert (GD) and nontarget (NT) in Fig. 8*C*]. CHD2 KD reduced the expression of each gene in hMGEs in our prior RNA-seq analysis, and expression of all three genes was also reduced in hMGEs upon CHD2 KO, suggesting that CHD2 could directly or indirectly regulate their expression (Fig. 8*D*).

Since NKX2-1 and CHD2 coassociate with these genomic locations, we tested whether they could regulate the expression of the putative CREs by luciferase reporter assay in hMGEs. Reporter expression from the *ZIC1* and *SPRY1* CREs was induced by NKX2-1 OE, while luciferase expression from the *PAX2* CRE was instead repressed relative to basal levels from the empty minimal promoter vector and was not induced by NKX2-1 OE. These effects of NKX2-1 OE were lost in CREs upon mutation of the NKX2-1 consensus binding site (Fig. 8*E*). By contrast, in hMGEs generated from the CHD2-KO hESC line, NKX2-1 OE did not induce reporter expression driven by the *ZIC1* or *SPRY1* CREs (Fig. 8*F*). Together, these data support a role for NKX2-1 binding to these CREs in regulating gene expression and suggest that CHD2 cobinding to some NKX2-1–activated CREs may facilitate transactivation of the associated genes during hMGE specification. This may account, at least in part, for the impaired expression of MGE and neuronal genes that we observed under conditions of CHD2 deficiency (Fig. 7). Together, these data support the utility of this model to define transcriptional events that underlie human MGE specification and cIN differentiation and to understand how their disruption alters cIN development and may contribute to neurodevelopmental disorders.

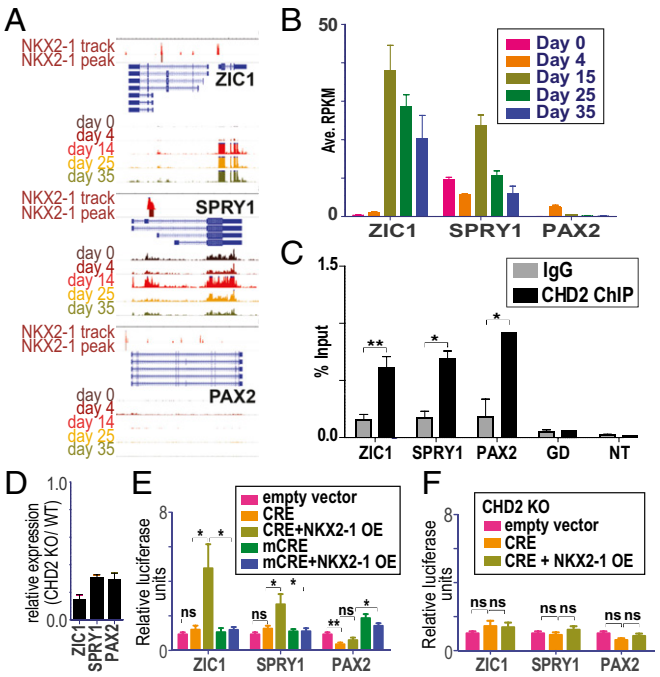

Fig. 8. Coregulation of gene expression by NKX2-1 and CHD2. (*A*) NKX2-1–bound peaks. (*B*) Associated genes exhibiting increased (*ZIC1*/*SPRY1*) or little (*PAX2*) expression from d0–35. (*C*) NKX2-1–bound peaks coenrich for CHD2; control amplicons (GD and NT) are not enriched. Shown is average enrichment; $n = 3$ independent biological replicates. (*D*) Expression of these genes is reduced in CHD2-KO hMGEs (d15). (*E*) NKX2-1 OE promotes reporter expression from the *ZIC1*/*SPRY1* CREs but not the *PAX2* CRE, which represses basal luciferase expression in hMGEs. Mutating the NKX2-1 consensus motif (mCRE) eliminates the response to NKX2-1 OE. (*F*) In CHD2-KO hMGEs, NKX2-1 OE does not promote *ZIC1* or *SPRY1* CRE-reporter expression. In *E* and *F*, the average fold change of RLUs versus the empty vector is shown; $n = 3$ or 4 per CRE, each performed in quintuplicate. For *C*, *E*, and *F*, $*P < 0.05$, $**P < 0.01$ (unpaired Student's t test); ns, not significant.

Discussion

Accelerated Differentiation of Mature cIN-Like Neurons from hESCs. Combining directed differentiation of human pluripotent cells with genome-wide analyses enables analysis of otherwise inaccessible regulatory events underlying aspects of human fetal development. Here, we began to elucidate gene regulatory networks that control specification of hMGEs and their differentiation into hcINs. We characterized molecular requirements for human cIN specification and differentiation by modifying directed differentiation approaches from prior work (17), with the goals of accelerating and improving the differentiation efficiency. Use of an EB step can accelerate hESC differentiation into mature neuronal cell types (26, 27). Therefore, we compared EB suspension versus monolayer culture conditions, defined optimal time windows for adding small-molecule signaling inhibitors and other supplements, and purified the progenitors by neural rosette selection. This promoted very efficient specification of NKX2-1–expressing hMGEs by d15 (80–90%), with most differentiating into hcINs that expressed general GABAergic, cIN, and mature MGE-derived cIN subtype markers (PV or SST) by d35. This approach yields higher percentages of hcINs expressing either PV or SST by 35 d than did prior protocols (16, 17).

At d35, negligible numbers of cells expressed the proliferative cell marker Ki-67 or alternate cell-lineage markers, indicating that this directed differentiation approach yields a largely postmitotic population of GABAergic, cIN-like neurons derived from MGE-like progenitors. These hcINs engrafted into the postnatal or adult murine brain and were still present more than 1 mo after transplantation. In vitro electrophysiological characterization demonstrated that these hcINs exhibit the expected electrophysiological properties: formation of voltage-gated and ligand-gated currents, action potential firing with most cells firing numerous spikes during prolonged depolarizing current pulses, and spontaneous inhibitory postsynaptic currents blocked by the GABA receptor antagonist bicuculline, resembling hcINs derived in prior work (16, 17). As previously described (16, 17), coculture of d35 hcINs with rat cortical astrocyte feeders elicited maturation of the action potential firing pattern and observation of frequent spontaneous inhibitory postsynaptic currents. These results corroborate prior findings that coculturing increases cIN functional maturation by an unknown mechanism (17).

Molecular Programs Regulating Specification and Differentiation of Human cIN-Like Neurons. In the mouse, ∼60% of cINs are MGE-derived, while ∼30% and ∼10% derive from the CGE or preoptic area, respectively (18). Although relative contributions to the human cIN population have been harder to ascertain, a significant proportion also appear to be MGE-derived (7, 18). Based upon molecular marker expression, this approach predominantly generates MGE-like progenitors: ∼80% of d15 cells express NKX2-1, an MGE-restricted marker, and other GE markers. We also observed molecular similarity between d15 hMGEs and MGEs in human 8- to 9-wk fetal brain. This protocol yields ∼70–80% GABAergic neurons, which express the MGE-derived cIN subtype markers *SST* or *PV*. By contrast, markers expressed by other cIN subtypes originating from the CGE or preoptic area (*CR*/*VIP*) (18, 28) were not induced. Together, these findings suggest that this protocol produces neurons resembling those derived from the MGE.

Transcriptome changes are much more limited from d25–35 than earlier, suggesting stabilization of the neuronal state. At this time, hcINs express both mature subtype markers (*SST* or *PV*) and other hallmarks of maturing neurons (e.g., enriched expression of genes involved in GABAergic synaptic neurotransmission). Therefore, while prior work describes stabilization of the transcriptome after d100 (19), some protocol modifications introduced here, such as *N*-[*N*-(3,5-difluorophenacetyl)-L-alanyl]-*S*-phenylglycine *t*-butyl ester (DAPT)-mediated inhibition of Notch signaling and neural rosette selection, enabled mature neurons to be isolated without coculturing by d35. This may enhance the utility of this system for modeling cell-intrinsic aspects of normal and altered cIN differentiation and function.

Integrating the Genome-Wide NKX2-1 Binding Profile with Enriched Gene Expression During cIN-Like Neuron Specification and Differentiation Reveals Direct Targets Involved in These Processes. In the mouse, NKX2-1 is required for MGE specification, acting at or near the top of regulatory networks controlling this process, while also promoting cIN differentiation (9–11). While NKX2-1 also exhibits MGE-restricted expression during fetal brain development in humans, its direct targets had not previously been defined. Here, we identified these targets by ChIP-seq analysis in hMGEs and integrated these data with hMGE- and hcIN-enriched expression. This revealed several prominent classes of direct targets through which NKX2-1 could promote MGE specification and cIN differentiation. In hMGEs, NKX2-1 associated with many TFs, including those with known roles in cIN development, in ventral telencephalic neural identity, or other aspects of neurodevelopment, or with no previously defined neurodevelopmental role. These findings support a major role for NKX2-1 in regulating the expression of TFs, which may comprise a transcriptional regulatory network for MGE specification. NKX2-1 also associates with many other gene classes, such as genes encoding natural antisense or long noncoding RNAs, which represent potential regulators of cIN development (for examples, see Table S2). Other classes of NKX2-1–associated genes were highly expressed in differentiating hcINs and control later cIN development and function. These include genes encoding GABA receptors, sodium and potassium channels, and other genes involved in synaptic output. These data support a continued role for NKX2-1 in directly controlling the expression of genes mediating cIN differentiation and function. However, as association does not demonstrate that NKX2-1 directly transactivates the expression of these genes, functional assays will be used to address this question in future work.

CHD2-Dependent Pathways in cIN Development and Function. Mutation of some NKX2-1–associated genes results in epilepsy, autism, and other neurodevelopmental disorders. We focused on one of these, a gene encoding the chromatin-remodeling enzyme CHD2. In humans, *CHD2* haploinsufficiency causes epileptic encephalopathies, pediatric disorders involving refractory seizures and cognitive decline (14). The CHD2-KO mouse model exhibits altered growth, hematopoietic differentiation, renal function, and tumor susceptibility but does not have apparent neurological phenotypes or exhibit seizures (29, 30). Therefore, we thought it would be informative to use hcINs to define molecular pathways sensitive to CHD2 deficiency and their relationship to NKX2-1.

We found that NKX2-1 promotes *CHD2* expression by binding a CRE at the *CHD2* promoter during MGE specification, while CHD2-deficient hMGE cells had reduced expression of many human epilepsy genes. These frequently encode sodium and potassium channels, while CHD2 loss altered hcIN sodium channel current activity and action potential thresholds. These data suggest that dysregulated channel expression and activity may alter hcIN function, contributing to epilepsy involving CHD2 deficiency. Notably, these results differ substantially from findings made in murine cortical excitatory neurons (31). In this work, shRNA KD of CHD2 during mouse cortical neurogenesis promoted differentiation of radial glial progenitors into TUBB3-expressing neurons. During hcIN specification and differentiation, we instead observed diminished and/or delayed production of TUBB3-expressing neurons and expression of synapse- and channel-related genes, which could reflect either assessment of different neurodevelopmental processes and/or species-specific differences.

Mechanisms of NKX2-1–Mediated Target Gene Transactivation. Cross-species comparisons revealed that 9.4% (hypergeometric P value = 3.4×10^{-27}) of human NKX2-1–associated genes associated with an NKX2-1–bound CRE in mouse MGEs (13). Many human-specific CREs and target genes were found, which may reflect both biological differences, including evolutionary divergence in developmental mechanisms, CRE locations, sequences, and genome organization, and the use of divergent models (dissected mouse tissue versus hESC-directed differentiation). Enriched consensus motifs for TF binding in human and mouse CREs also exhibited both similarities and differences: Mouse CREs were coenriched for Nkx, Lhx, Oct4, and E-Box motifs (13), with Lhx6 and Nkx2-1 motifs associated with genes activated during cIN differentiation. In human hMGEs, we likewise found NKX2-1 and LHX motif enrichment, but we did not observe OCT4 or E-BOX motifs and additionally found coenrichment for SOX2/3/6 motifs in 15–25% of the NKX2-1–bound peaks.

Sox and homeodomain TFs cobind CREs to regulate multiple aspects of neural development (32). For example, ventral neural tube patterning involves CRE co-occupancy by SOXB1 TFs (SOX1–3), which broadly activate neural transcription, and by NKX2-2 and NKX6-1, which repress alternate fates to control regional patterning (33–35). During human fetal development, SOX2 and NKX2-1 are coexpressed by MGE progenitors until postconception week 28, supporting potential cofunction (7, 8). Relative to murine development, the generation of more cINs over an extended period could favor the use of coactivators such as SOX2/3, which promote MGE progenitor maintenance. Iterative occupancy of the same binding sites by SOX2, SOX3, and SOX11 promotes gene expression during neural fate acquisition (36). Similarly, here SOX2/3 might cooperate with NKX2-1 to promote the formation or maintenance of MGE progenitors, with SOX6 regulating later expression in cINs. Consistent with a potential role, SOX2/3 levels peak in d4 ventral neuroectoderm and are diminished by d35, while SOX6 expression initiates at d15 and continues in cINs. Twenty percent of these NKX2-1–bound peaks intersected with SOX2-binding profiles defined previously for human neural progenitors, and SOX2 and NKX2-1 cobound a set of CREs at neural development-related genes that increase expression during MGE specification.

We also defined a potential role for CHD2 as a cofactor in NKX2-1–dependent gene regulation. A subset of NKX2-1–associated genes had diminished expression following CHD2 deficiency. CHD2 coassociated with NKX2-1 at CREs for several of these genes in hMGEs, while CHD2 KO interfered with CRE-driven reporter activation by NKX2-1. Both NKX2-1 and CHD2 deficiencies can cause epilepsy in humans and/or mice, and CHD2 KO in hcINs altered their electrophysiological properties and dysregulated the

expression of genes encoding sodium and potassium channels that are mutated to cause human epilepsy. Therefore, it would be interesting to test whether any of these epilepsy genes is coordinately regulated by NKX2-1 and CHD2 binding to the same CRE. Together, these data demonstrate the utility of this directed differentiation approach to elaborate transcriptional events underlying human MGE specification and cIN differentiation, to define direct targets and mechanisms by which TFs and chromatin-modifying activities contribute to this process, and to study how its dysregulation may contribute to neurodevelopmental disorders.

Methods

hESC Maintenance and Differentiation. H9 and HES3 hESC lines were grown under feeder-free conditions on Matrigel (Corning) in mTeSR1 (STEMCELL Technologies). Cortical excitatory and inhibitory neuronal differentiation was performed by modification of prior protocols (*SI Methods*) (16, 17). Experiments adhered to protocols (#12-002) approved by the Washington University hESC Research Oversight Committee. As this work was designated "nonhuman subjects research" by Washington University's Institutional Review Board, informed consent was not required.

Immunocytochemistry. Primary antibodies are given in Table S3, and ICC and neurite outgrowth analysis is described in *SI Methods*.

Electrophysiology and cIN Transplantation. d35 PSA–NCAM–purified, SYN–eGFP–expressing hcINs were used for transplantation and electrophysiology as described in *SI Methods*. Transplantation experiments were performed by the Animal Surgery Core at Washington University School of Medicine using protocols approved by the Institutional Animal Care and Use Committee of Washington University in St. Louis.

RNA-Seq and RT-qPCR Analysis. Total RNA was collected from H9 hESCs and H9-derived neural derivatives using the NucleoSpin RNA II kit (Takara). Illumina library construction, sequencing, data analysis, and RT-qPCR are described in detail in *SI Methods*. qPCR primer sequences are given in Table S4.

ChIP/ChIP-Seq. hMGEs were used for NKX2-1 ChIP by modification of standard methods (*SI Methods*).

FACS. HES3 or H9 hESC-derived neurons were dissociated with Accutase (STEMCELL Technologies), and a single-cell suspension was prepared. Cells were washed once each with PBS and FACS buffer (2% BSA, 1 mM EDTA in PBS) and were resuspended in FACS buffer. For detailed protocols, see *SI Methods*.

CHD2 KD and KO in hESCs. For KD, hESCs were stably transduced with validated lentiviral shRNA expression vectors directed against CHD2. CRISPR/Cas9 technology was used to generate clonal hESC lines with biallelic disruption of *CHD2*. For detailed information and shRNA/gRNA sequences, see *SI Methods*.

ACKNOWLEDGMENTS. We thank Matheus Victor and Andrew Yoo for assisting in cIN transplantations and for the SYN–GFP plasmid; David Mu for the NKX2-1 vector (Addgene); and Andrew Yoo and Harrison W. Gabel for constructive suggestions on the manuscript. This project was supported by NIH Grants GM66815 (to K.L.K.) and NS3088 (to J.E.H.); March of Dimes Grant 1-FY13-413 (to K.L.K.); grants from the American Epilepsy Society, the McDonnell Center for Cellular and Molecular Neurobiology at Washington University (WU), and the WU Center for Regenerative Medicine (CRM); WU Institute of Clinical and Translational Sciences Grant UL1 TR000448; the WU Animal Surgery Core; and the WU Gene Technology Access Center (supported by Siteman Cancer Center Grants CA91842 and UL1 TR000448). K.M. was supported by a Postdoctoral Fellowship from the WU CRM, and E.M.A.L. was supported by a National Institute of General Medical Science T32 Training Grant.

1. Kessaris N, Magno L, Rubin AN, Oliveira MG (2014) Genetic programs controlling cortical interneuron fate. *Curr Opin Neurobiol* 26:79–87.
2. Arber C, Li M (2013) Cortical interneurons from human pluripotent stem cells: Prospects for neurological and psychiatric disease. *Front Cell Neurosci* 7:10.
3. Powell EM (2013) Interneuron development and epilepsy: Early genetic defects cause long-term consequences in seizures and susceptibility. *Epilepsy Curr* 13:172–176.
4. Kepecs A, Fishell G (2014) Interneuron cell types are fit to function. *Nature* 505: 318–326.
5. Taniguchi H (2014) Genetic dissection of GABAergic neural circuits in mouse neocortex. *Front Cell Neurosci* 8:8.
6. Clowry GJ (2015) An enhanced role and expanded developmental origins for gamma-aminobutyric acidergic interneurons in the human cerebral cortex. *J Anat* 227: 384–393.
7. Hansen DV, et al. (2013) Non-epithelial stem cells and cortical interneuron production in the human ganglionic eminences. *Nat Neurosci* 16:1576–1587.
8. Arshad A, et al. (2016) Extended production of cortical interneurons into the third trimester of human gestation. *Cereb Cortex* 26:2242–2256.
9. Sussel L, Marin O, Kimura S, Rubenstein JL (1999) Loss of Nkx2.1 homeobox gene function results in a ventral to dorsal molecular respecification within the basal telencephalon: Evidence for a transformation of the pallidum into the striatum. *Development* 126:3359–3370.
10. Xu Q, Cobos I, De La Cruz E, Rubenstein JL, Anderson SA (2004) Origins of cortical interneuron subtypes. *J Neurosci* 24:2612–2622.
11. Butt SJB, et al. (2008) The requirement of Nkx2-1 in the temporal specification of cortical interneuron subtypes. *Neuron* 59:722–732.
12. Breedveld GJ, et al. (2002) Mutations in TITF-1 are associated with benign hereditary chorea. *Hum Mol Genet* 11:971–979.
13. Sandberg M, et al. (2016) Transcriptional networks controlled by NKX2-1 in the development of forebrain GABAergic neurons. *Neuron* 91:1260–1275.
14. Carvill GL, et al. (2013) Targeted resequencing in epileptic encephalopathies identifies de novo mutations in CHD2 and SYNGAP1. *Nat Genet* 45:825–830.
15. Goulburn AL, et al. (2011) A targeted NKX2.1 human embryonic stem cell reporter line enables identification of human basal forebrain derivatives. *Stem Cells* 29: 462–473.
16. Nicholas CR, et al. (2013) Functional maturation of hPSC-derived forebrain interneurons requires an extended timeline and mimics human neural development. *Cell Stem Cell* 12:573–586.
17. Maroof AM, et al. (2013) Directed differentiation and functional maturation of cortical interneurons from human embryonic stem cells. *Cell Stem Cell* 12:559–572.
18. Wonders CP, Anderson SA (2006) The origin and specification of cortical interneurons. *Nat Rev Neurosci* 7:687–696.
19. Close JL, et al. (2017) Single-cell profiling of an in vitro model of human interneuron development reveals temporal dynamics of cell type production and maturation. *Neuron* 93:1035–1048.e5.
20. Iyer NR, Huettner JE, Butts JC, Brown CR, Sakiyama-Elbert SE (2016) Generation of highly enriched V2a interneurons from mouse embryonic stem cells. *Exp Neurol* 277: 305–316.
21. Flandin P, et al. (2011) Lhx6 and Lhx8 coordinately induce neuronal expression of Shh that controls the generation of interneuron progenitors. *Neuron* 70:939–950.
22. Nóbrega-Pereira S, et al. (2008) Postmitotic Nkx2-1 controls the migration of telencephalic interneurons by direct repression of guidance receptors. *Neuron* 59:733–745.
23. Muhr J, Andersson E, Persson M, Jessell TM, Ericson J (2001) Groucho-mediated transcriptional repression establishes progenitor cell pattern and neuronal fate in the ventral neural tube. *Cell* 104:861–873.
24. Zhou C, et al. (2016) Comprehensive profiling reveals mechanisms of SOX2-mediated cell fate specification in human ESCs and NPCs. *Cell Res* 26:171–189.
25. Harada A, et al. (2012) Chd2 interacts with H3.3 to determine myogenic cell fate. *EMBO J* 31:2994–3007.
26. Muratore CR, Srikanth P, Callahan DG, Young-Pearse TL (2014) Comparison and optimization of hiPSC forebrain cortical differentiation protocols. *PLoS One* 9:e105807.
27. Zhang SC, Wernig M, Duncan ID, Brüstle O, Thomson JA (2001) In vitro differentiation of transplantable neural precursors from human embryonic stem cells. *Nat Biotechnol* 19:1129–1133.
28. Miyoshi G, et al. (2010) Genetic fate mapping reveals that the caudal ganglionic eminence produces a large and diverse population of superficial cortical interneurons. *J Neurosci* 30:1582–1594.
29. Marfella CGA, et al. (2006) Mutation of the SNF2 family member Chd2 affects mouse development and survival. *J Cell Physiol* 209:162–171.
30. Nagarajan P, et al. (2009) Role of chromodomain helicase DNA-binding protein 2 in DNA damage response signaling and tumorigenesis. *Oncogene* 28:1053–1062.
31. Shen T, Ji F, Yuan Z, Jiao J (2015) CHD2 is required for embryonic neurogenesis in the developing cerebral cortex. *Stem Cells* 33:1794–1806.
32. Bailey PJ, et al. (2006) A global genomic transcriptional code associated with CNS-expressed genes. *Exp Cell Res* 312:3108–3119.
33. Nishi Y, et al. (2015) A direct fate exclusion mechanism by sonic hedgehog-regulated transcriptional repressors. *Development* 142:3286–3293.
34. Kutejova E, Sasai N, Shah A, Gouti M, Briscoe J (2016) Neural progenitors adopt specific identities by directly repressing all alternative progenitor transcriptional programs. *Dev Cell* 36:639–653.
35. Oosterveen T, et al. (2013) SoxB1-driven transcriptional network underlies neural-specific interpretation of morphogen signals. *Proc Natl Acad Sci USA* 110:7330–7335.
36. Bergsland M, et al. (2011) Sequentially acting Sox transcription factors in neural lineage development. *Genes Dev* 25:2453–2464.